IJMMM International Journal of Minerals, Metallurgy and Materials 矿物冶金与材料学报（英文版）

Preparation of CIP@TiO_2 composite with broadband electromagnetic wave absorption properties

Qiang Su, Hanqun Wang, Yunfei He, Dongdong Liu, Xiaoxiao Huang, and Bo Zhong

INTERNATIONAL JOURNAL OF
Minerals, Metallurgy and Materials

Volume 31, Number 1, January 2024
Page 197

Research Article https://doi.org/10.1007/s12613-023-2707-5

Preparation of CIP@TiO_2 composite with broadband electromagnetic wave absorption properties

Qiang Su[1], *Hanqun Wang*[1], *Yunfei He*[1], *Dongdong Liu*[1], *Xiaoxiao Huang*[2], *and Bo Zhong*[1],✉

1) School of Materials Science and Engineering, Harbin Institute of Technology, Weihai, Weihai 264209, China
2) School of Materials Science and Engineering, Harbin Institute of Technology, Harbin 150001, China
(Received: 20 April 2023; revised: 10 July 2023; accepted: 11 July 2023)

Abstract: Scholars aim for the improved impedance matching (Z) of materials while maintaining their excellent wave absorption properties. Based on the hydrolysis characteristics of isopropyl titanate, a simple preparation process for the coating of carbonyl iron powder (CIP) with TiO_2 was designed. Given the TiO_2 coating, the Z of the CIP@TiO_2 composite was adjusted well by decreasing the dielectric constant. Moreover, the interfacial polarization of CIP@TiO_2 was enhanced. Ultimately, the electromagnetic-wave (EMW) absorption property of the CIP@TiO_2 composite was improved substantially, the minimum reflection loss reached −46.07 dB, and the effective absorption bandwidth can reach 8 GHz at the composite thickness of 1.5 mm. Moreover, compared with CIP, the oxidation resistance of CIP@TiO_2 showed remarkable improvement. The results revealed that the oxidation starting temperature of CIP@TiO_2 was about 400°C, whereas the uncoated CIP had an oxidation starting temperature of approximately 250°C. Moreover, the largest oxidation rate temperature of CIP@TiO_2 increased to around 550°C. This work opens up a novel strategy for the production of high-performance EMW absorbers via structural design.

Keywords: carbonyl iron@titanium dioxide; electromagnetic-wave absorption; impedance matching; oxidation resistance

1. Introduction

The electromagnetic pollution generated by wide applications of electronic devices not only influences the regular operations of sensitive electrical equipment but also threatens human health. The application of electromagnetic-wave (EMW) absorption materials can be used to effectively tackle electromagnetic pollution in daily production and life [1]. Electromagnetic radiation can be absorbed efficiently by EMW absorption materials and converted to heat energy. Thus, they have been an important concern and widely developed in recent years [2–4].

Given its excellent temperature stability, low vortex loss, and affordable production, carbonyl iron powder (CIP) has become one of the frequently used EMW absorption materials [5–6]. In general, magnetic materials follow Snoek's law [7]:

$$(\mu_s - 1) f_r = \frac{2}{3}\gamma \times 4\pi M_s \tag{1}$$

where γ represents the gyromagnetic ratio, M_s indicates the saturation magnetization, $\mu_s - 1$ refers to the static susceptibility, and f_r denotes the relaxation frequency. Moreover, $\mu_s - 1$ and f_r correspond to the maximum of the imaginary part of the complex permeability μ''. Materials with a large M_s tend to have a high μ''. Compared with traditional ferrite magnetic absorbing materials, CIP has a higher saturation magnetization and a Snoek limit at higher frequencies and can be applied to a wider frequency range of EMW absorption materials [8–9]. Although the application of CIP in the field of EMW absorption has numerous advantages, it also faces several limitations when used as a single-EMW absorption material. For example, the strong oxidation of CIP leads to easy oxidation in high-temperature environments and easy corrosion in high-humidity environments [10], and its poor impedance matching (Z) often results in impedance mismatch, which prevents the EMW from penetrating the material effectively [11]. Therefore, CIP can be applied widely in the EMW absorption field by adjusting its Z and enhancing its oxidation resistance and corrosion resistance while maintaining its excellent absorption performance. Surface coating is a common method to improve the EMW absorption property of CIP [12–13]. It can create a core–shell structure that isolates CIP from oxygen and increases oxidation and corrosion resistance. The coated material can also be used to adjust the electromagnetic parameters of CIP to improve its Z and increase its interface polarization and relaxation. The coated CIP can generate multiple scattering to the incident electromagnetic EMW because of its unique core–shell structure, which promotes the enhancement of its EMW absorption performance. The typically used coating materials include SiO_2 [14–15], MnO_2 [16–17], $BaTiO_3$ [18–19], BN [20–21], C [22–23], polymethyl methacrylate [24–25], poly-

✉ Corresponding author: Bo Zhong E-mail: zhongbo@hit.edu.cn

aniline [26–27], TiO_2 [28–31], and so on. Among these coated materials, TiO_2 has garnered the most interest due to its strong isolation, simple coating process management, efficient base material protection, and affordable price. Xu *et al.* [28] successfully synthesized the core–shell structure carbon@titanium dioxide composite microspheres with a wrinkled surface through a three-step method and built up the relationship between the TiO_2 layer thickness and the EMW absorption property. The minimum reflection loss (RL_{min}) reached −49.21 dB at the thickness of 2 mm, and the corresponding effective absorption bandwidth (EAB) was 5.27 GHz. Liu *et al.* [29] coupled polyaniline (PANI) to the porous TiO_2 anchored on magnetic graphene via a two-step strategy combining *in situ* polymerization and a hydrothermal process. The results indicated that magnetic graphene@PANI was completely covered by porous TiO_2 with random orientations, and the saturation magnetization of the composite was 19.2 $A\cdot m^2\cdot kg^{-1}$; the RL_{min} of the composite was up to −45.4 dB. Qiao *et al.* [30] fabricated the Ni-embedded TiO_2/C core–shell ternary nanofibers using the combined methods of electrospinning and subsequent thermal treatment. The surface of the carbon nanofibers (diameter: 200 nm) was coated with a rough and wrinkled layer of TiO_2, and metallic Ni nanoparticles with a size of 20–30 nm were uniformly embedded in the nanofiber matrix. The ternary nanofibers with a molar ratio of 4:1 between TiO_2 and metallic Ni exhibited an excellent maximum EAB of 6.7 GHz at the thickness of 2.6 mm, with the RL_{min} reaching −74.5 dB at 2.0 mm. Chen *et al.* [31] synthesized multifunctional composite microspheres with a $Co_{20}Ni_{80}$ core and anatase TiO_2 shells ($Co_{20}Ni_{80}@TiO_2$) by combining a solvothermal reaction and a calcination process. The $Co_{20}Ni_{80}@TiO_2$ core–shell particles (CoNi@TiO_2) with a well-defined core size of 500 nm demonstrated a remarkable wide-band electromagnetic shielding performance of up to 6.2 GHz (10.0–16.2 GHz; −10 dB) within 2–18 GHz. All these studies and results demonstrate TiO_2 as an ideal material to satisfy the requirements of EMW absorption. Thus, scholars should further investigate the excellent process of coating CIP with TiO_2.

Based on the hydrolysis characteristics of isopropyl titanate (TTIP), the CIP@TiO_2 composite was prepared by a simple sol–gel method in aqueous ethanol. The CIP@TiO_2 had a core–shell structure in which CIP was the core, and TiO_2 served as the shell covering the surface of CIP. The morphology and structure of the CIP@TiO_2 composite were characterized by an X-ray diffractometer (XRD), scanning electron microscope (SEM), and transmission electron microscope (TEM), and the performance of EMW absorption was tested using a vector network analyzer. In addition, we investigated the influence of CIP oxidation resistance by TiO_2 coating. The test results showed that the core–shell CIP@TiO_2 had excellent EMW absorption properties and oxidation resistance.

2. Experimental

2.1. Materials

The CIP (average particle size of 9.7 μm) was supplied by Xindun Alloy Welding Material Spraying Co., Ltd. Isopropyl titanate (TTIP) (95%) was purchased from Shanghai Maclin Biochemical Technology Co., Ltd. Ethyl alcohol (analytical reagent, 99.7%) was acquired from Yantai Shuangshuang Chemical Co., Ltd.

2.2. Preparation of CIP@TiO_2

To describe the synthesis process visibly, we provide details for the preparation of the CIP@TiO_2 EMW absorption composite (Fig. 1) as follows.

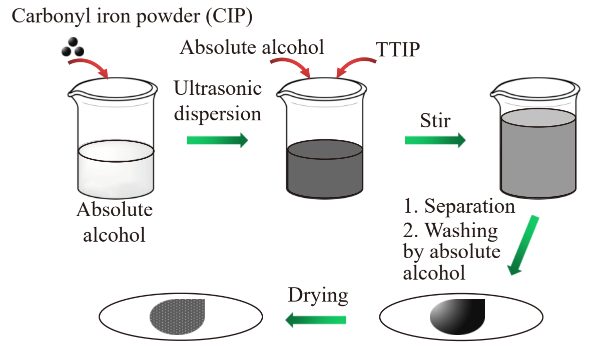

Fig. 1. Schematic of the CIP@TiO_2 composite preparation process.

First, 1.0 g CIP was ultrasonically dispersed in 20 mL of anhydrous ethanol. Then, 1.0–3.0 mL TTIP and 30 mL anhydrous ethanol were added, and the mixture was stirred at 500 r/min for 180 min. The product was separated, washed with anhydrous ethanol, and dried at 60°C for 12 h. Finally, the dried product was ground and collected. In this investigation, four groups were set for the comparison experiments and named Ti-0, Ti-1, Ti-2, and Ti-3 based on the different amounts of TTIP addition. Table 1 shows the amount of reagents added in each experiment.

Table 1. Reagent addition amount in each experiment

Experimental group	CIP / g	TTIP / mL
Ti-0	1.0	0
Ti-1	1.0	1.0
Ti-2	1.0	2.0
Ti-3	1.0	3.0

2.3. Characterization

An XRD (DX-2700, Dandong Haoyuan Instruments Co., Ltd.) was used for the phase and structural analysis of the EMW absorption composite. The scanning range was from 10° to 90°. The internal morphology of the absorption materials was observed using an SEM (Merlin Compact, Zeiss), and the surface elements were analyzed by energy dispersive spectroscopy (EDS) spectral analysis. A TEM (JEM-2100, JEOL) was used to investigate the sample characteristics of the EMW absorption composites. The sample morphology and high-resolution image were observed with bright-field and phase-contrast imaging, respectively. Diffraction patterns were acquired by selected electron diffraction operations. A vibrating sample magnetometer (Lake-Shore 7404, Lake-Shore) was used to analyze the magnetic properties of the samples. The high-temperature oxidation process of the samples was analyzed using a thermal analyzer (DTAN-60H, SHIMADZU).

To explore the EMW absorption properties of the CIP@TiO$_2$ EMW composite, we used the EMW vector network analyzer (Agilent N5245A, Agilent) to test the EMW absorption properties. The samples were prepared by uniformly mixing the CIP@TiO$_2$ powder and molten paraffin at the mass ratio of 4:1 and cold pressing the obtained mixed colloid in the mold into circular samples with outer and inner diameters of 7.0 and 3.04 mm, respectively.

3. Results and discussion

3.1. Synthesis mechanism of CIP@TiO$_2$

Fig. 2 shows the synthesis mechanism of CIP@TiO$_2$. First, the TTIP with four isopropoxy functional groups was hydrolyzed into the hydrolysis product, and the hydrolysis product was condensed with the hydroxyl group on the CIP surface to construct the underlying molecular layer. The free hydrolysis products that contained the hydroxyl groups continuously reacted with the basal molecular layer, which allowed the TiO$_2$ shell on the CIP surface to grow incessantly and eventually form the intact TiO$_2$ shell [32]. Moreover, Wei *et al.* [33] investigated the kinetics of the TTIP hydrolysis reaction. They observed that the hydrolysis of TTIP mainly occurs in the following stages: First, the C–O bond dissociated to form Ti(O·)(OC$_3$H$_7$)$_3$. Second, the Ti–O or C–O bond was broken to form TiO(OC$_3$H$_7$)$_2$ or Ti(O·)(OH)(OC$_3$H$_7$)$_2$. Third, C–O cleavage preferred TiO(OC$_3$H$_7$)$_2$, which produced TiO(OH)(OC$_3$H$_7$) and TiO(O·)(OC$_3$H$_7$). These species either combined immediately to form clusters or continually released the remaining –O$_x$C$_3$H$_y$ groups to create small intermediates, such as TiO(OH)$_2$, Ti·O(OH), and Ti··(OH)$_2$. In addition, early clusters can be observed before the first TiO$_2$ molecule was observed in the simulation.

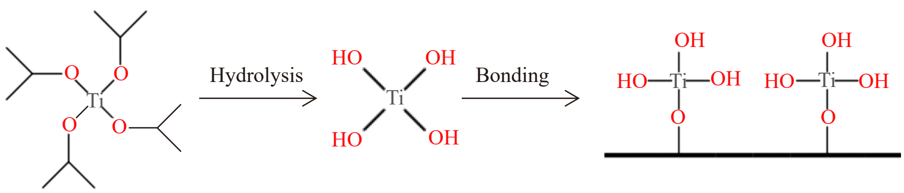

Fig. 2. Bonding mode of the TiO$_2$ coating process.

3.2. Phase and morphology characterization

Fig. 3 presents the XRD image of the composite. The spectra of Ti-0 showed three diffraction peaks at 44.67°, 65.02°, and 82.33°, which correspond to the (110), (200), and (211) crystal planes of α-Fe, respectively (JCPDS No. 06-0696) [34]. As displayed in the XRD image of CIP@TiO$_2$(Ti-2), the position and intensity of the three diffraction peaks remained unchanged after TiO$_2$ coating compared with Ti-0. This finding preliminarily proved the amorphous structure and low content of the coated TiO$_2$ shell. Other studies also obtained similar results [35–37].

Fig. 4(a) and (b) shows the SEM images of CIP (Ti-0) and CIP@TiO$_2$ (Ti-2), respectively. The figure reveals that the uncoated CIP had a spherical structure with a smooth surface, and the surface of CIP@TiO$_2$ featured a coated layer composed of various irregular small particles. The EDS element analysis of CIP@TiO$_2$ was performed to further investigate

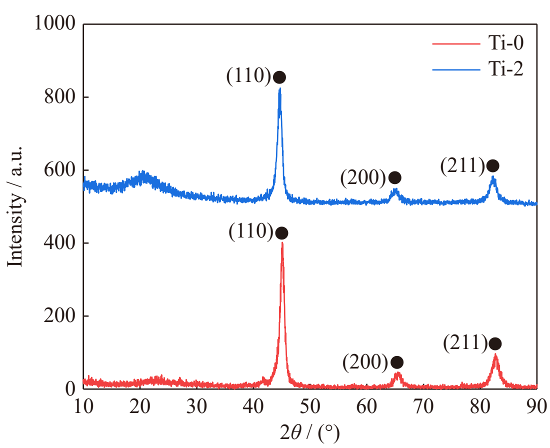

Fig. 3. XRD spectra of Ti-0 and Ti-2.

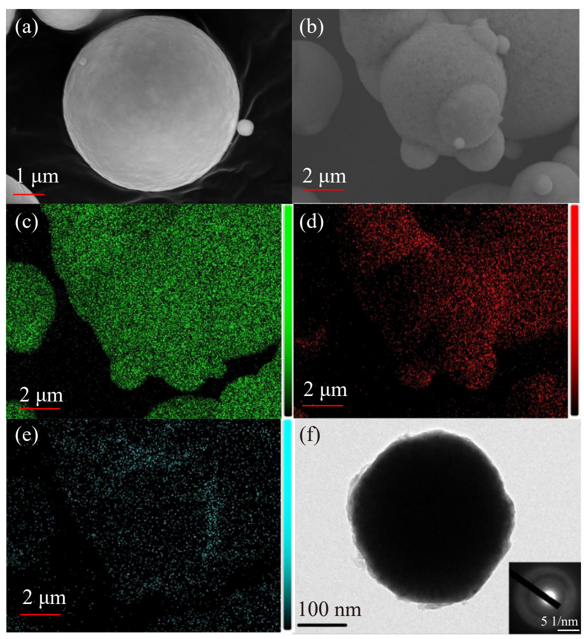

Fig. 4. (a) SEM image of CIP (Ti-0), (b) SEM image of CIP@TiO$_2$ (Ti-2), (c) distribution of Fe in CIP@TiO$_2$ (Ti-2), (d) distribution of O in CIP@TiO$_2$, (e) distribution of Ti in CIP@TiO$_2$, and (f) TEM image of CIP@TiO$_2$ (Ti-2) (illustration is the selected electron diffraction image of shell area).

the element distribution in the CIP@TiO_2 composite. The test results revealed that the main element, that is, Fe, was uniformly distributed in CIP@TiO_2, where Ti and O were also present (Fig. 4(c)–(e)), and Ti was uniformly dispersed on the surface of Fe. However, O was distributed in some dense areas because of the characteristic of the CIP preparation process, and some O atoms were evenly dispersed in CIP [38], overlapping with the O in TiO_2 to form partially dense regions. The TEM test further confirmed the structure of CIP@TiO_2, and as shown in Fig. 4(f), the core–shell structure of CIP@TiO_2 can be observed distinctly. The black sphere at the center is the CIP core, and the translucent thin outer shell is the coated TiO_2 shell. Fig. 4(f) also shows the selected electron diffraction on the shell area. The results revealed no evident single-crystal or polycrystal characteristics, which indicated the amorphous structure that corresponded to the XRD findings.

3.3. Microwave absorption performance

Reflection loss (RL), which is described using electromagnetic characteristics, such as frequency and thickness, in accordance with transmission line theory, can be used to define the EMW absorption property. The specific formulas are shown in the following equations:

$$\mathrm{RL\,(dB)} = 20\lg|(Z_{in} - Z_0)/(Z_{in} + Z_0)| \tag{2}$$

$$Z_0 = \sqrt{\frac{\mu_0}{\varepsilon_0}} \tag{3}$$

$$Z = |Z_{in}/Z_0| = \sqrt{|\mu_r/\varepsilon_r|}\tanh\left[\mathrm{j}(2\pi f d/c)\sqrt{\mu_r\varepsilon_r}\right] \tag{4}$$

where Z_0 represents the impedance of the air, Z_{in} denotes the impedance of the material, f indicates the frequency, d refers to the thickness of the material, c is the speed of light, ε_r corresponds to the complex dielectric constant ($\varepsilon_r = \varepsilon' - \mathrm{j}\cdot\varepsilon''$), and μ_r represents the magnetic permeability ($\mu_r = \mu' - \mathrm{j}\cdot\mu''$) [39–42]. Fig. 5 shows the RL values of different samples. The RL_{min} reached −46.07 dB at 5.04 GHz and a thickness of 3.1 mm for Ti-1 and −22.77 dB at 3.28 GHz and a thickness of 4 mm for Ti-0. Furthermore, the effective frequency bandwidth of the RL below −10 dB (over 90% electromagnetic absorption) was 8 GHz at the thickness of 1.5 mm for Ti-2, and such a value is larger than that of Ti-0. Compared with CIP, the EMW absorption intensity and material coating thickness of CIP@TiO_2 exhibited considerable improvement. Moreover, a small difference was observed in the EMW absorption property between Ti-2 and Ti-3. Such a finding was due to the bonding mechanism of hydrolysates, which limited the shell thickness and thus resulted in similar TiO_2 shell thicknesses of Ti-2 and Ti-3.

To further investigate the EMW absorption property of CIP and the CIP@TiO_2 composites, we presented the calculated RL values of Ti-0 and Ti-2 in three dimensional (3D) diagrams. Fig. 6(a) and (b) shows the RL performance of CIP and the CIP@TiO_2 composites, respectively, under the influence of frequency and thickness. The CIP without TiO_2 coating exhibited a low RL in the frequency range of 2–6 GHz and thickness range of 3–4 mm. Meanwhile, the CIP@TiO_2

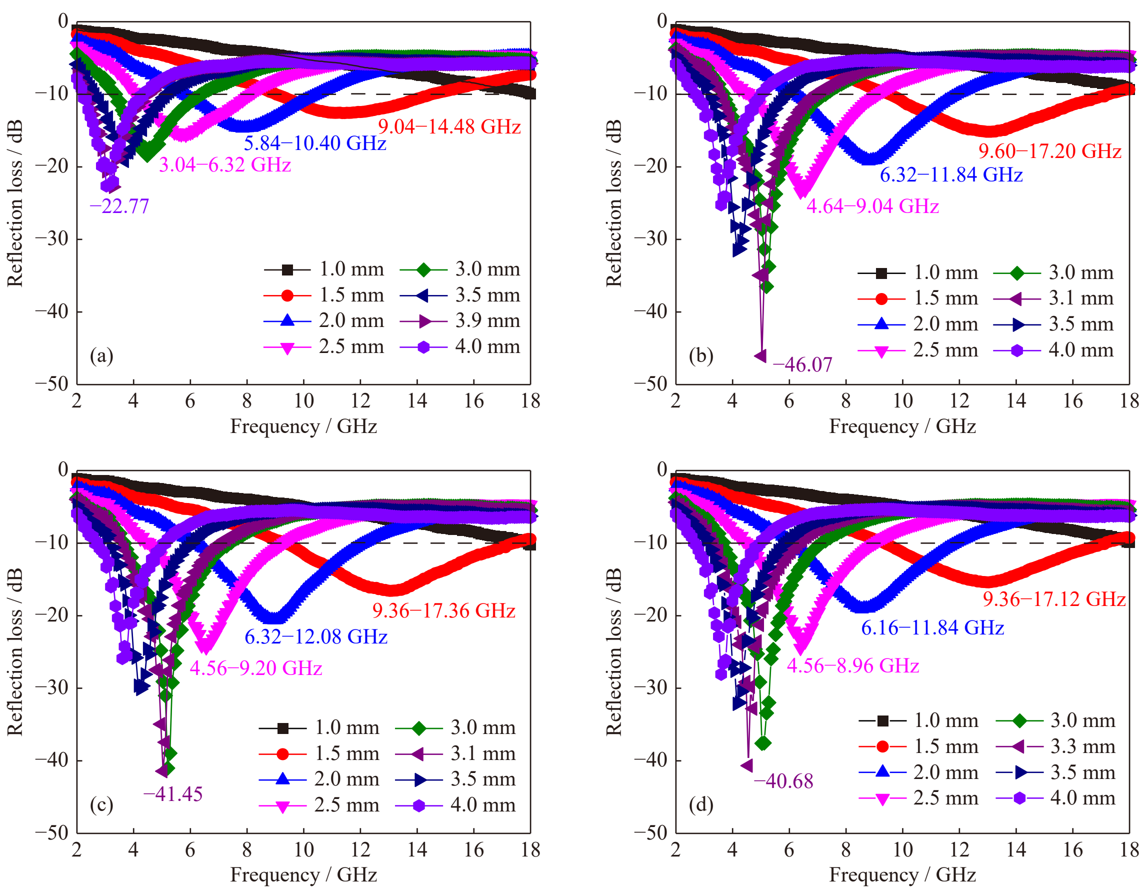

Fig. 5. RL values with different TiO_2 contents of CIP@TiO_2 composite: (a) Ti-0, (b) Ti-1, (c) Ti-2, and (d) Ti-3.

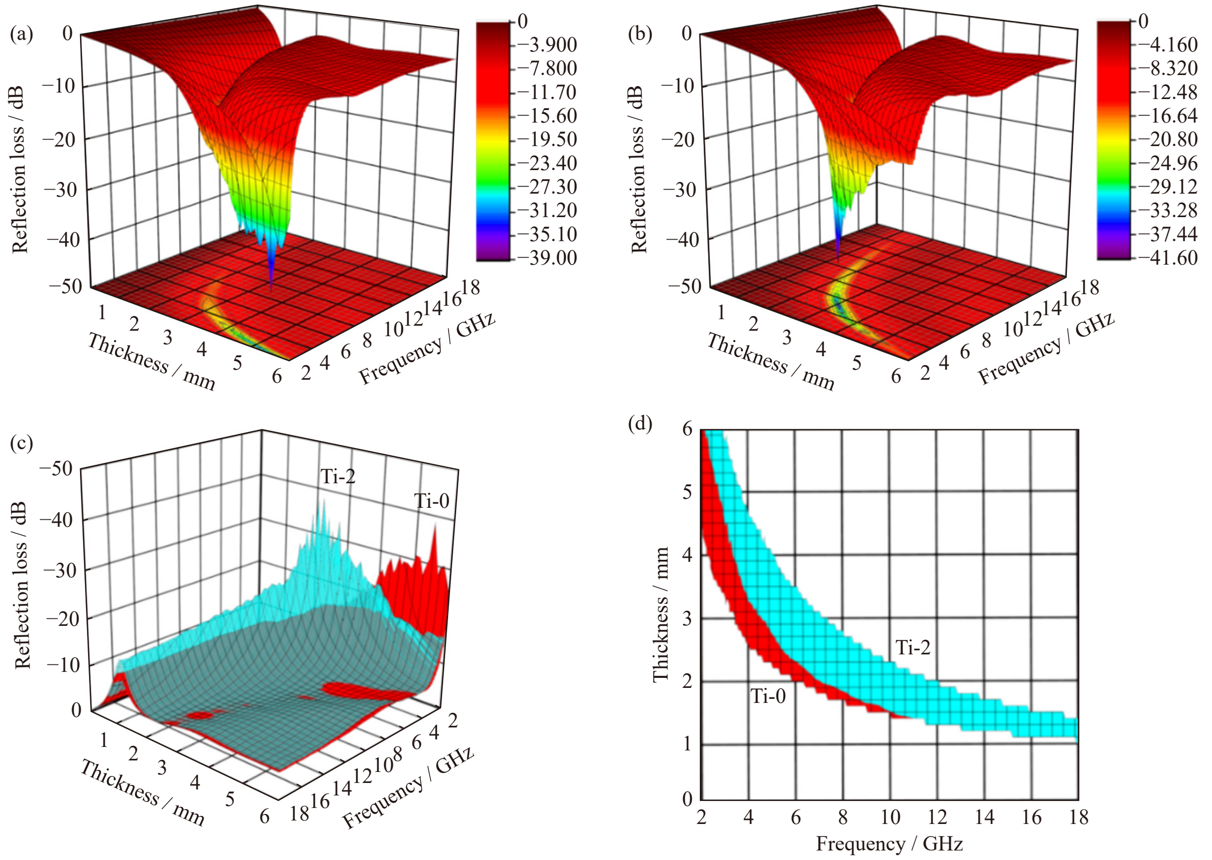

Fig. 6. 3D color maps of the RL values of (a) Ti-0 and (b) Ti-2 at different thicknesses and frequencies. (c, d) Comparison of RL values of Ti-0 (red) and Ti-2 (blue), respectively.

showed a low RL in the frequency range of 6–10 GHz and thickness range of 2–3 mm. Fig. 6(c) and (d) displays the EMW absorption performance difference between CIP and CIP@TiO$_2$, respectively. After CIP has been coated by TiO$_2$, the absorption peak of RL moved to the direction of high frequency and low thickness, and the effective absorption region shifted to the area with smaller thickness and higher frequency.

Fig. 7 displays the EMW absorption performance change of CIP and CIP@TiO$_2$, with the increased content of TTIP, the absorption peak position at 1.5 mm remained almost unchanged, and the positions of the 2.0 and 2.5 mm groups showed similar trends; that is, they increased first and then decreased in a very small range. Moreover, for the same component of the absorbing material, with the increase in thickness, the RL$_{min}$ peak position moved to low frequencies. This phenomenon can be explained by the quarter-wavelength model. It can be described by the following equation [14]:

$$t_m = nc/\left(4f_m\sqrt{|\varepsilon_r||\mu_r|}\right), (n = 1,3,5,\ldots) \quad (5)$$

where t_m and f_m represent the thickness and peak frequency, respectively. ε_r and μ_r mean the complex permittivity and permeability at f_m, respectively. When the values of ε_r and μ_r are fixed, for the satisfaction of the formula requirements, the RL$_{min}$ peak position of the composite material must shift to lower frequencies with the increase in sample thickness. Ti-1, Ti-2, and Ti-3 revealed small differences between their

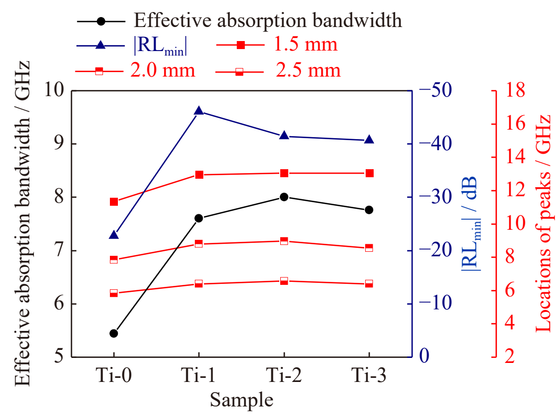

Fig. 7. Variation in CIP and CIP@TiO$_2$ absorption performances.

EMW absorption because the bonding mechanism of hydrolysates limited the shell thickness, which resulted in similar TiO$_2$ shell thicknesses in the three groups of experiments.

Fig. 8(a)–(c) shows the frequency dependences of the ε', ε'', and $\tan\delta_\varepsilon$ (dielectric loss angle tangent value) of CIP and CIP@TiO$_2$ composites. Compared with the uncoated CIP (Ti-0), given the introduction of TiO$_2$, the ε' and ε'' of CIP@TiO$_2$ were reduced, and the $\tan\delta_\varepsilon$ of CIP@TiO$_2$ was reduced considerably. Moreover, the stability of the ε' (small difference in the range of 2–18 GHz) benefited the improvement of the Z of the material [43]. Fig. 8(d)–(f) illustrates the μ', μ'', and $\tan\delta_\mu$ of CIP and CIP@TiO$_2$ composites, respectively. When TiO$_2$ was coated on the CIP surface, compared

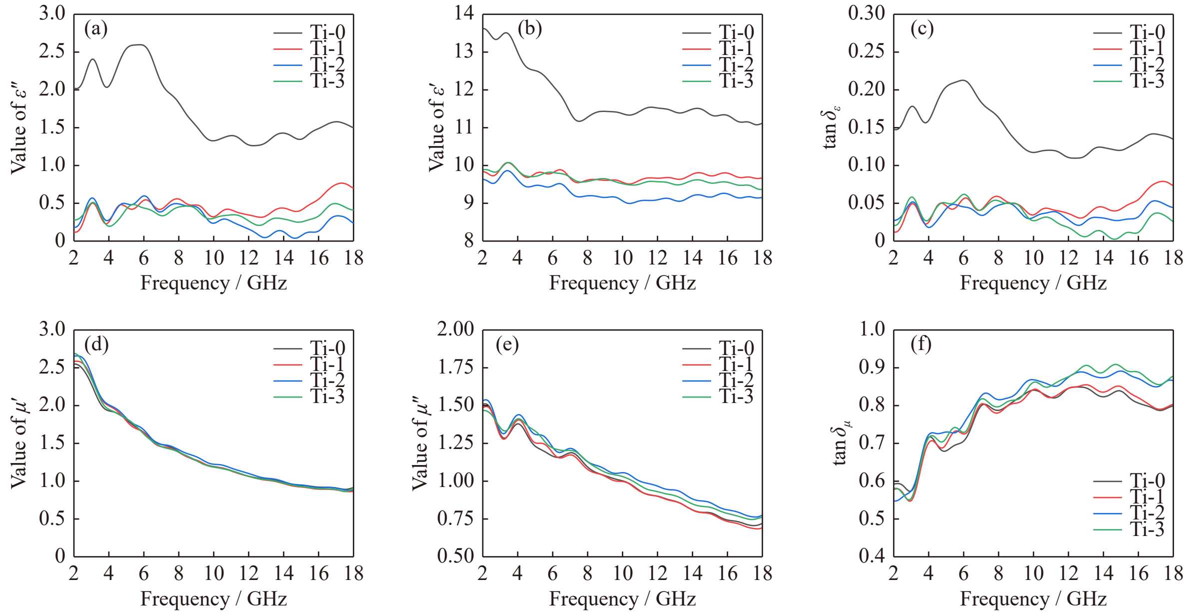

Fig. 8. EMW absorption parameters of composites: (a) dielectric real part (ε'), (b) dielectric imaginary part (ε''), (c) dielectric loss angle ($\tan\delta_\varepsilon$), (d) magnetic real part (μ'), (e) magnetic imaginary part (μ''), and (f) magnetic loss angle ($\tan\delta_\mu$).

with those of the CIP, the μ', μ'', and $\tan\delta_\mu$ of the CIP@TiO_2 composite exhibited less variation. This finding indicates that the TiO_2 shell had a negligible influence on the magnetic properties of the CIP.

Fig. 9 shows the Z values of CIP and CIP@TiO_2 composites with different thicknesses. In general, the Z_{in} of materials with a good Z should be close to the Z_0. Therefore, the Z_{in}/Z_0 of EMW absorption material close to 1 implies a desirable Z [44]. As shown in Fig. 9(a), the thick CIP can achieve an ideal Z and peak at low frequencies. Ti-1, Ti-2, and Ti-3 exhibited the same tendency. Their input impedances were closer to 1 compared with that of CIP (Fig. 9(b)–(d)), although some curves of lower thicknesses crossed the optimum Z_{in}/Z_0 value line. Compared with that of CIP, the Z of

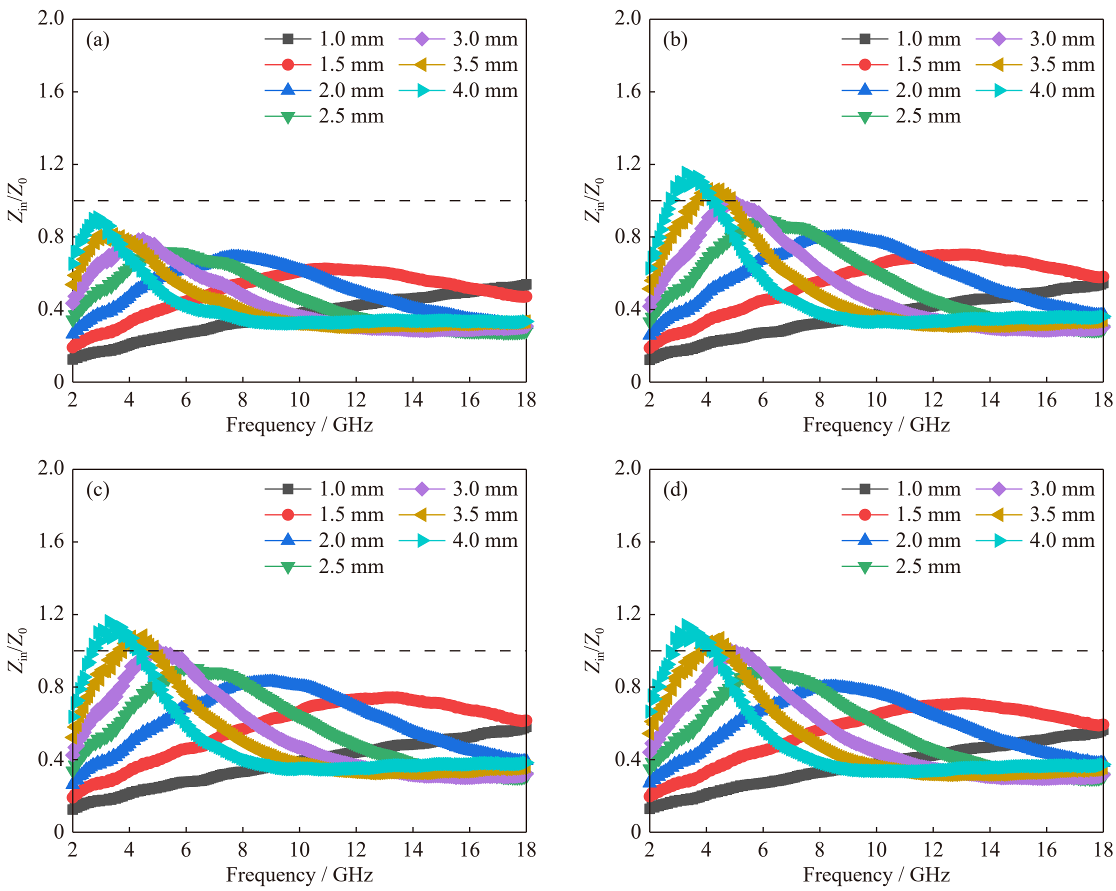

Fig. 9. Frequency dependences of the RL of absorbers with different thicknesses: (a) Ti-0, (b) Ti-1, (c) Ti-2, and (d) Ti-3.

CIP@TiO_2 was optimized evidently. However, as the bonding mechanism of hydrolysates limited the shell thickness, Ti-1, Ti-2, and Ti-3 showed similar Z, which provided the opportunity to acquire the ideal Z_{in}/Z_0 value with a thin layer, which is beneficial for applications of EMW absorption materials. For instance, as shown in Fig. 9(a), the original CIP must be at least 4 mm thick to obtain the optimal value, and Fig. 9(c) shows that this thickness may be reduced to 3 mm with TiO_2 coating. In addition, when the frequencies corresponding to the optimal Z_{in}/Z_0 values were broadened, the better Z_{in}/Z_0 values corresponded to wider and thinner absorbers. The CIP coated by TiO_2 is anticipated to be an excellent thin EMW absorption material.

In general, Z and attenuation constant play a major role in outstanding EMW absorbers, and dielectric and magnetic losses are the main types of losses [45]. CIP is a typical magnetic absorption material; thus, its EMW absorption mechanism is mainly magnetic loss, including natural resonance and eddy vortex loss [46]. However, a portion of EMW can enter CIP, and the majority of EMW is reflected because of the poorly matched input and free space impedances. Although CIP has a strong EMW attenuation capability, it still shows poor EMW absorption characteristics. The Z relationship between CIP and free space improved considerably due to the existence of a TiO_2 shell, which enhanced the overall input impedance of CIP@TiO_2 (Fig. 10). Therefore, more incident EMW can penetrate the CIP interior. Moreover, given the heterogeneous interface between CIP and TiO_2, heterogeneous interface polarization occurred, and the EMW energy was converted to thermal energy through interfacial polarization relaxation [45,47]. These mechanisms that resulted in the formation of CIP@TiO_2 composites indicate excellent EMW absorption characteristics.

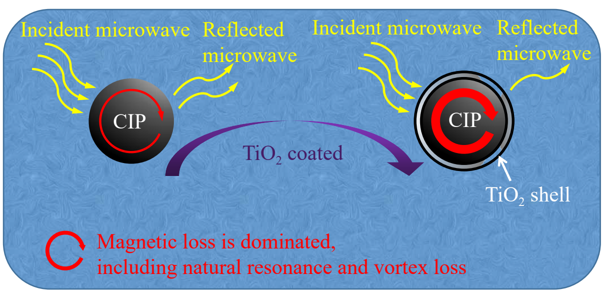

Fig. 10. Absorption mechanisms of CIP and CIP@TiO_2.

Fig. 11(a) shows the changes in the weight of CIP@TiO_2 with the gradual increase in temperature from the thermogravimetric (TG) analysis. The oxidation starting temperature of uncoated CIP (Ti-0) was approximately 250°C. Thereafter, the weight continuously increased with the increase in the temperature and finally reached a stable value. CIP@TiO_2 showed a similar trend as CIP (Ti-0), but the initial oxidation temperature increased to around 400°C. When the temperature reached 650°C, the weight of the four experimental groups remained almost unchanged; that of Ti-0 was retained at 138%, and those of Ti-1 to Ti-3 were at 140%. This phenomenon was caused by the transformation of the original amorphous TiO_2 into a slightly denser rutile-type TiO_2 [48]. Fig. 11 (b) shows the curves of the weight change rate with temperature by the derivative TG (DTG) analysis. The figure also reveals that pure CIP (Ti-0) had the largest weight change rate at ~500°C, which indicates that the CIP oxidation rate was the fastest at this temperature. However, given the introduction of TiO_2, the largest oxidation rate temperature of CIP@TiO_2 increased to around 550°C. This test indicated that the introduction of TiO_2 coating improved the initial conditions of high-temperature oxidation, delayed the occurrence of high-temperature oxidation, and substantially improved the oxidation resistance of CIP.

4. Conclusions

In summary, based on the hydrolysis characteristics of TTIP, a simple preparation process of CIP coated with TiO_2 was proposed. The TTIP was used as a titanium source, the surface modification process of CIP coated with TiO_2 in anhydrous ethanol was realized, and the CIP@TiO_2 composite was obtained. The CIP@TiO_2 composite has the following characteristics.

(1) Attributing to the coated TiO_2, the ε', ε'' and $\tan\delta_\varepsilon$ of CIP@TiO_2 decreased considerably, but the μ', μ'', and $\tan\delta_\mu$ of CIP@TiO_2 were almost unchanged. The test results showed that CIP@TiO_2 had a better Z compared with the CIP.

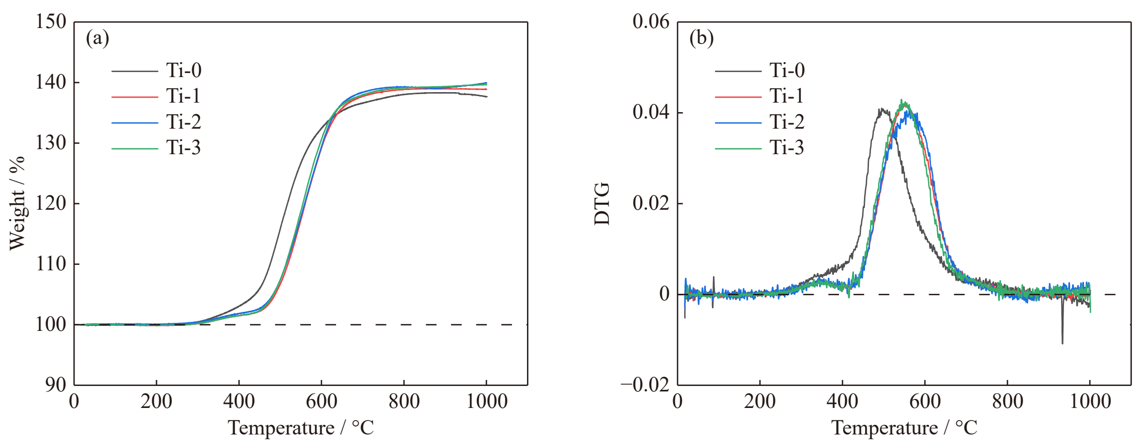

Fig. 11. TG (a) and DTG curves (b) of CIP@TiO_2.

(2) The heterogeneous interface polarization between CIP and TiO_2 further enhanced the EMW absorption property of CIP@TiO_2. Therefore, the CIP@TiO_2 composite exhibited desirable *Z* and excellent attenuation capacity for EMW. The EMW absorption test revealed that the RL_{min} of CIP@TiO_2 can reach −46.07 dB, and the EAB was 8 GHz when its thickness was 1.5 mm. The EMW absorption property of CIP@TiO_2 was improved evidently in terms of EMW absorption intensity, material coating thickness, and EAB.

(3) Given the coated TiO_2 on the CIP surface, the oxidation starting temperature of CIP@TiO_2 was about 400°C, and that of uncoated CIP (Ti-0) was approximately 250°C. Moreover, the largest oxidation rate temperature of CIP@TiO_2 increased to around 550°C.

This work opens up a novel strategy for the manufacture of high-performance EMW absorbers through structure design.

Acknowledgements

This work was financially supported by the National Natural Science Foundation of China (No. 51872058) and the Supporting Program for Innovation Team of Outstanding Youth in Colleges and Universities of Shandong Province (No. 2020KJA005).

Conflict of Interest

The authors declare that they have no known competing financial interests or personal relationships that could have appeared to influence the work reported in this paper.

References

[1] X.F. Xu, G.Z. Wang, G.P. Wan, *et al*., Magnetic Ni/graphene connected with conductive carbon nano-onions or nanotubes by atomic layer deposition for lightweight and low-frequency microwave absorption, *Chem. Eng. J.*, 382(2020), art. No. 122980.

[2] Z.G. Gao, K. Yang, Z.H. Zhao, *et al*., Design principles in MOF-derived electromagnetic wave absorption materials: Review and perspective, *Int. J. Miner. Metall. Mater.*, 30(2023), No. 3, pp. 405-427.

[3] S.J. Zhang, J.Y. Li, X.T. Jin, *et al*., Current advances of transition metal dichalcogenides in electromagnetic wave absorption: A brief review, *Int. J. Miner. Metall. Mater.*, 30(2023), No. 3, pp. 428-445.

[4] H. Sun, R.C. Che, X. You, *et al*., Cross-stacking aligned carbon-nanotube films to tune microwave absorption frequencies and increase absorption intensities, *Adv. Mater.*, 26(2014), No. 48, p. 8120.

[5] Y.F. Zhang, A.M. Bu, Y. Xiang, *et al*., Rapid synthesis of scaly SiO_2 coating on flake carbonyl iron powders by plasma electrolysis, *Mater. Sci. Eng. B*, 262(2020), art. No. 114703.

[6] Q.L. Chen, L.Y. Li, Z.L. Wang, Y.C. Ge, C.S. Zhou, and J.H. Yi, Synthesis and enhanced microwave absorption performance of CIP@ SiO_2@$Mn_{0.6}Zn_{0.4}Fe_2O_4$ ferrite composites, *J. Alloys Compd.*, 779(2019), p. 720.

[7] Y.T. Zhao, L. Liu, J.N. Han, W.H. Wu, and G.X. Tong, Effective modulation of electromagnetic characteristics by composition and size in expanded graphite/Fe_3O_4 nanoring composites with high Snoek's limit, *J. Alloys Compd.*, 728(2017), p. 100.

[8] H. Xie, Y.Y. Zhou, Z.W. Ren, X. Wei, S.P. Tao, and C.Q. Yang, Enhancement of electromagnetic interference shielding and heat-resistance properties of silver-coated carbonyl iron powders composite material, *J. Magn. Magn. Mater.*, 499(2020), art. No. 166244.

[9] P.C. Ji, G.Z. Xie, N.Y. Xie, *et al*., Fabrication and microwave absorption properties of the flaky carbonyl iron/FeSiAl composite in S-band, *J. Mater. Sci. Mater. Electron.*, 29(2018), No. 6, p. 4711.

[10] X.L. Guo, Z.J. Yao, H.Y. Lin, *et al*., Epoxy resin addition on the microstructure, thermal stability and microwave absorption properties of core–shell carbonyl iron@epoxy composites, *J. Magn. Magn. Mater.*, 485(2019), p. 244.

[11] X.Q. Chen, Z. Wu, Z.L. Zhang, L.Y. Heng, S. Wang, and Y.H. Zou, Impedance matching for omnidirectional and polarization insensitive broadband absorber based on carbonyl iron powders, *J. Magn. Magn. Mater.*, 476(2019), p. 349.

[12] L.Y. Yang, L.H. Yin, C.Q. Hong, S. Dong, C. Liu, and X.H. Zhang, Strong and thermostable hydrothermal carbon coated 3D needled carbon fiber reinforced silicon–boron carbonitride composites with broadband and tunable high-performance microwave absorption, *J. Colloid Interface Sci.*, 582(2021), p. 270.

[13] J.J. Ding, L. Wang, Y.H. Zhao, *et al*., Boosted interfacial polarization from multishell TiO_2 @Fe_3O_4 @PPy heterojunction for enhanced microwave absorption, *Small*, 15(2019), No. 36, art. No. e1902885.

[14] L.Q. Yue, B. Zhong, L. Xia, T. Zhang, Y.L. Yu, and X.X. Huang, Three-dimensional network-like structure formed by silicon coated carbon nanotubes for enhanced microwave absorption, *J. Colloid Interface Sci.*, 582(2021), p. 177.

[15] H.Q. Wang, M. Wang, X.C. Zhang, *et al*., A new type of catalyst allows carbonyl iron powder to be coated with SiO_2 for tuned microwave absorption, *Surf. Interfaces*, 21(2020), art. No. 100755.

[16] Z. Komeily-Nia, M. Montazer, S.S.S. Aye, and B. Nasri-Nasrabadi, A practical approach to load CuO/MnO_2 core/shell nanostructures on textiles through *in situ* wet chemical synthesis, *Colloids Surf. A: Physicochem. Eng. Aspects*, 583(2019), art. No. 123998.

[17] M.T. Qiao, X.F. Lei, Y. Ma, *et al*., Facile synthesis and enhanced electromagnetic microwave absorption performance for porous core–shell Fe_3O_4@MnO_2 composite microspheres with lightweight feature, *J. Alloys Compd.*, 693(2017), p. 432.

[18] R.L. Gao, Z.H. Wang, G. Chen, X.L. Deng, W. Cai, and C.L. Fu, Influence of core size on the multiferroic properties of $CoFe_2O_4$@$BaTiO_3$ core shell structured composites, *Ceram. Int.*, 44(2018), p. S84.

[19] G.M. Shi, Y.F. Li, L. Ai, and F.N. Shi, Two step synthesis and enhanced microwave absorption properties of polycrystalline $BaTiO_3$ coated Ni nanocomposites, *J. Alloys Compd.*, 680(2016), p. 735.

[20] B. Zhong, Y.J. Cheng, M. Wang, *et al*., Three dimensional hexagonal boron nitride nanosheet/carbon nanotube composites with light weight and enhanced microwave absorption performance, *Compos. Part A: Appl. Sci. Manuf.*, 112(2018), p. 515.

[21] Q. Su, D.D. Liu, C.Y. Wang, L. Xia, X.X. Huang, and B. Zhong, Graphene/BN/Fe/BN nanocomposites for highly efficient electromagnetic wave absorption, *ACS Appl. Nano Mater.*, 5(2022), No. 10, p. 15902.

[22] D.T. Kuang, L.Z. Hou, S.L. Wang, *et al*., Facile synthesis of Fe/Fe_3C–C core–shell nanoparticles as a high-efficiency microwave absorber, *Appl. Surf. Sci.*, 493(2019), p. 1083.

[23] C. Fu, D.W. He, Y.S. Wang, and X. Zhao, Facile synthesis and microwave absorption performance of coated carbon nanotubes by porous Fe_3O_4@C nanorods, *Synth. Met.*, 248(2019), p. 76.

[24] W.Y. Jang, S. Mallesh, S.B. Lee, and K.H. Kim, Microwave absorption properties of core–shell structured FeCoNi@PMMA filled in composites, *Curr. Appl. Phys.*, 20(2020), No. 4, p. 525.
[25] A.A. Mahani, S. Motahari, and V. Nayyeri, Electromagnetic and microwave absorption characteristics of PMMA composites filled with a nanoporous resorcinol formaldehyde based carbon aerogel, *RSC Adv.*, 8(2018), No. 20, p. 10855.
[26] H.Y. Yan, Y.Q. Fu, X.M. Wu, X.X. Xue, C. Li, and L. Zhang, Core–shell structured $NaTi_2(PO_4)_3$@polyaniline as an efficient electrode material for electrochemical energy storage, *Solid State Ion.*, 336(2019), p. 95.
[27] A.F. Zhu, H.L. Xing, Q. Fan, X.L. Ji, and P. Yang, Conductive polyaniline coated on aluminum substrate as bi-functional materials with high-performance microwave absorption and low infrared emissivity, *Synth. Met.*, 271(2021), art. No. 116640.
[28] J. Xu, Z.H. Liu, J.Q. Wang, *et al*., Preparation of core–shell C@TiO_2 composite microspheres with wrinkled morphology and its microwave absorption, *J. Colloid Interface Sci.*, 607(2022), p. 1036.
[29] P.B. Liu, Y. Huang, J. Yan, and Y. Zhao, Magnetic graphene@PANI@porous TiO_2 ternary composites for high-performance electromagnetic wave absorption, *J. Mater. Chem. C*, 4(2016), No. 26, p. 6362.
[30] J. Qiao, X. Zhang, C. Liu, *et al*., Facile fabrication of Ni embedded TiO_2/C core–shell ternary nanofibers with multicomponent functional synergy for efficient electromagnetic wave absorption, *Compos. Part B: Eng.*, 200(2020), art. No. 108343.
[31] C. Chen, Q.H. Liu, H. Bi, W.B. You, W. She, and R.C. Che, Fabrication of hierarchical TiO_2 coated $Co_{20}Ni_{80}$ particles with tunable core sizes as high-performance wide-band microwave absorbers, *Phys. Chem. Chem. Phys.*, 18(2016), No. 38, p. 26712.
[32] P. Arora, A. Fermah, J.K. Rajput, H. Singh, and J. Badhan, Efficient solar light-driven degradation of Congo red with novel Cu-loaded Fe_3O_4@TiO_2 nanoparticles, *Environ. Sci. Pollut. Res. Int.*, 24(2017), No. 24, p. 19546.
[33] J.L. Wei, A. Ostadhossein, S.Q. Li, and M. Ihme, Kinetics for the hydrolysis of $Ti(OC_3H_7)_4$: A molecular dynamics simulation study, *Proc. Combust. Inst.*, 38(2021), No. 1, p. 1433.
[34] D.N. Chen, K.L. Li, H.Y. Yu, *et al*., Effects of secondary particle size distribution on the magnetic properties of carbonyl iron powder cores, *J. Magn. Magn. Mater.*, 497(2020), art. No. 166062.
[35] C.W. Zhang, Y. Peng, T.L. Zhang, W.B. Guo, Y. Yuan, and Y.B. Li, *In situ* dual-template method of synthesis of inverse-opal Co_3O_4@TiO_2 with wideband microwave absorption, *Inorg. Chem.*, 60(2021), No. 23, p. 18455.
[36] M. He, Q. Liao, Y.M. Zhou, *et al*., Lightweight TiO_2@C/carbon fiber aerogels prepared from $Ti_3C_2T_x$/cotton for high-efficiency microwave absorption, *Langmuir*, 38(2022), No. 3, p. 945.
[37] D.Q. Zhang, Y.F. Xiong, J.Y. Cheng, *et al*., Construction of low-frequency and high-efficiency electromagnetic wave absorber enabled by texturing rod-like TiO_2 on few-layer of WS_2 nanosheets, *Appl. Surf. Sci.*, 548(2021), art. No. 149158.
[38] S.K.M. Jamari, N.A. Nordin, U. Ubaidillah, S.A.A. Aziz, S.A. Mazlan, and N. Nazmi, Enhancement of the rheological properties of magnetorheological elastomer via polystyrene-grafted carbonyl iron particles, *J. Appl. Polym. Sci.*, 138(2021), No. 34, art. No. 50860.
[39] X. Li, C.Y. Wen, L.T. Yang, R.X. Zhang, Y.S. Li, and R.C. Che, Enhanced visualizing charge distribution of 2D/2D MXene/MoS_2 heterostructure for excellent microwave absorption performance, *J. Alloys Compd.*, 869(2021), art. No. 159365.
[40] C.W. Qiang, J.C. Xu, Z.Q. Zhang, *et al*., Magnetic properties and microwave absorption properties of carbon fibers coated by Fe_3O_4 nanoparticles, *J. Alloys Compd.*, 506(2010), No. 1, p. 93.
[41] Z. Zhang, H.Q. Zhao, W.H. Gu, L.J. Yang, and B.S. Zhang, A biomass derived porous carbon for broadband and lightweight microwave absorption, *Sci. Rep.*, 9(2019), No. 1, art. No. 18617.
[42] Y.L. Yu, M. Wang, Y.Q. Bai, *et al*., Tuning the inner hollow structure of lightweight amorphous carbon for enhanced microwave absorption, *Chem. Eng. J.*, 375(2019), art. No. 121914.
[43] Y. Liu, Y.N. Li, K.D. Jiang, G.X. Tong, T.X. Lv, and W.H. Wu, Controllable synthesis of elliptical Fe_3O_4@C and Fe_3O_4/Fe@C nanorings for plasmon resonance-enhanced microwave absorption, *J. Mater. Chem. C*, 4(2016), No. 30, p. 7316.
[44] X.X. Sun, M.L. Yang, S. Yang, *et al*., Ultrabroad band microwave absorption of carbonized waxberry with hierarchical structure, *Small*, 15(2019), No. 43, art. No. 1902974.
[45] M. Yu, Y. Huang, X.D. Liu, X.X. Zhao, W.Q. Fan, and K.H. She, *In situ* modification of MXene nanosheets with polyaniline nanorods for lightweight and broadband electromagnetic wave absorption, *Carbon*, 208(2023), p. 311.
[46] K.S. Sista, S. Dwarapudi, D. Kumar, G.R. Sinha, and A.P. Moon, Carbonyl iron powders as absorption material for microwave interference shielding: A review, *J. Alloys Compd.*, 853(2021), art. No. 157251.
[47] X.D. Liu, S. Zhang, M. Yu, *et al*., WS_2 nanosheets anchored on N-doped carbon fibers for superior electromagnetic wave absorption, *Chem. Eng. J.*, 465(2023), art. No. 142932.
[48] C.M. Gao, T. Wei, Y.Y. Zhang, *et al*., A photoresponsive rutile TiO_2 heterojunction with enhanced electron–hole separation for high-performance hydrogen evolution, *Adv. Mater.*, 31(2019), No. 8, art. No. 1806596.